Using μSR to investigate the vortex lattice in high-temperature superconductors

C. M. Aegerter[(1)], *S. L. Lee [(2)]
[(1)]Physik-Institut der Universität Zürich, CH-8057 Zürich, Switzerland.
[(2)]School of Physics and Astronomy, University of St. Andrews, St. Andrews, Fife KY16 9SS, UK.

October 22, 1997

*Corresponding author

Abstract

We review some of the properties of the vortex lattice in type II superconductors and the use of muon spin rotation (μSR) to investigate high temperature superconducting oxides. As a microscopic probe of the field distribution inside the bulk of materials, μSR is shown to be a powerful tool with which to study the magnetic properties of superconductors. We also discuss how understanding the complex phenomenology of the vortex lattice in these materials is necessary in order to correctly determine fundamental parameters of the superconducting state.

1 Introduction

Muon spin rotation (μSR) is a unique tool with which to investigate the magnetic properties of superconductors. This is because the muon acts as a *microscopic* probe of the field distribution within the *bulk* of the sample. In the mixed state of type II superconductors the applied magnetic field penetrates the sample in the form of vortices of superconducting electrons, each of which carries one quantum of magnetic flux $\phi_0 = h/2e$, where h is Planck's constant and e is the charge of an electron. In conventional superconductors these are line vortices, or *flux lines*, but in high-temperature superconductors (HTSC) they may adopt more exotic forms. It is the arrangement of these vortices which give rise to the distribution of magnetic fields in the sample. In HTSC, the unconventional vortex arrangments may lead to interesting phenomena such as the vortex-glass and the vortex-liquid state. The understanding of the properties of the flux line lattice are of importance to possible applications of superconductors. In the mixed state the passage of a current through the bulk of the sample will exert a Lorentz force on the flux vortices, and the resulting motion will lead to a dissipation of energy and hence loss of perfect conductivity. This motion is hindered by the presence of material defects, which act as pinning sites. Above a certain critical current the force exerted on the vortices is sufficient for them to break free and for flux flow to occur. Applications of HTSC are mainly hindered by their relatively poor critical currents, which are due to low pinning strengths in these samples. By performing μSR studies on HTSC we can, however, gain insights into the pinning mechanisms and strengths in these materials, and how they could be improved. The study of the behaviour of vortices also yields fundamental parameters of a superconducting system, such as the penetration depth and the coherence length. From systematic studies of these parameters, insight can be gained about the pairing mechanism and symmetry of the system, which is still an open question for the HTSC copper oxides.

We now give a short synopsis of our review: Although the basic principles of μSR have already been discussed by E. Roduner in this volume [1], in Section 2 we will address some special questions regarding μSR important to our data analysis. We then go on in Section 3 to present some considerations on the nature of type II superconductors and some basic properties of anisotropic flux line lattices, which are especially important in the discussion of HTSC. In this context we will also show how the spatial distribution of the magnetic field yields the field probability distribution, which is the quantity measured in μSR. We also discuss the effects that different types of disorder have on the field distribution. Some experimental limitations are discussed which relate to the study of samples having very long penetration depths or anisotropies, after which we review some of the novel transitions in highly anisotropic HTSC. Due to the importance of the pinning strength in HTSC to applications, in Section 4 we will present a short treatment of this topic, and some related μSR measurements.

2 Principles of μSR

For the basic principles of μSR we refer to the introductory article by E. Roduner [1], where it is shown that in a transverse field experiment, the muon spin polarisation can be measured from the asymmetry of the μSR signal. Monitoring the positron decay distribution as a function of time, one can therefore observe the time dependence of the muon polarisation vector. If the muons are distributed randomly over the sample cross-section interesecting the beam, the time dependence of the polarisation vector is just given by the Larmor precession of the muon in the local field at the muon site. From this one is then able to show that, in transverse geometry,

$$\mathcal{F}(P^+(t)) = \frac{2\pi}{\gamma_\mu} p\left(-\frac{\omega}{\gamma_\mu}\right) \tag{1}$$

where $\mathcal{F}$ denotes the Fourier transformation, p(B) is the field probability distribution ($p(B') := \langle \delta(B(\vec{r}) - B') \rangle$) and γ_μ is the gyromagnetic ratio of the muon. The fourier transform of the muon spin polarisation is thus a direct measure of the field probability distribution. Since the asymmetry of the μSR signal measures this spin polarisation, we are able to probe directly the field distribution in the sample by Fourier transform μSR. In practice, conventional Fourier transform methods exhibit several problems. Significant noise in the time signal at long times, due to finite count rates, is distributed over the whole of frequency space. Furthermore, only a finite time window is available to the experiment, leading to further aberrations in the frequency spectra. While the effects of these may be minimised by suitable data treatment, we apply an alternative technique based on a maximum entropy algorithm [2]. This leads to significant improvements in the quality of the Fourier transforms. In the algorithm used we maximise $S - \lambda\chi^2$, where S is the information entropy and λ a Lagrange multiplier [2]. This leads to the most uniform frequency distribution consistent with the time spectrum, and no prior assumptions on the form of the distribution are needed. In the investigation of superconductors the Fourier

transformed μSR approach is especially fruitful, since the field probability distribution does not have a simple analytic form, which could be included in a time-domain fit. This use of the maximum entropy technique in Fourier transform μSR thus allows us to investigate various properties of the vortex lattice directly, since the field probability distribution $p(B)$ is closely related to the spatial distribution of flux lines $B(r)$. We will now discuss some properties of vortex lattices and their effects on $B(r)$ and hence on $p(B)$.

3 Field distributions of vortex lattices

The electronic and magnetic properties of type I superconductors are described by the phenomenological theory developed by H. and F. London. On the basis of a macroscopic order parameter for the whole sample they proposed two equations which could describe perfect conductivity (cf. equation 2) and diamagnetic screening (cf. equation 3).

$$\frac{d\vec{j_s}}{dt} = \frac{1}{\mu_0 \lambda^2}\vec{E} \tag{2}$$

$$\vec{\nabla} \times \vec{j_s} = -\frac{1}{\mu_0 \lambda^2}\vec{B} \tag{3}$$

where $\lambda = \sqrt{\frac{m_s}{\mu_0 e_s^2 n_s}}$ is called the London penetration depth, with m_s being the mass, e_s the charge and n_s the density of the superconducting carriers. The perfect diamagnetic screening, also called Meissner effect, is the main magnetic property of type I superconductors. In type II superconductors, however, the spatial variation of the order parameter, neglected in the London theory, has to be taken into account. This requires the more elaborate Ginzburg-Landau theory, capable of describing flux lines. The existence of flux lines can be justified by considering the phase boundary energy between the superconducting and the normal state in an external field. For type II superconductors, it is energetically favorable for the magnetic field to penetrate into the superconductor above a certain critical field $\mu_0 H_{c_1} = \frac{\Phi_0}{4\pi\lambda^2} ln \frac{\lambda}{\xi}$ in the form of flux lines, each carrying one quantum of flux. The flux line consists of a vortex of supercurrents surrounding a core of normal (non-superconducting) electrons. Due to interaction of the supercurrents which make up the flux lines, the vortices repel one another and hence form a regular hexagonal lattice. When the density of flux lines is high enough for their normal cores to overlap, superconductivity is destroyed. This happens above the upper critical field $\mu_0 H_{c_2} = \frac{\Phi_0}{2\pi\xi^2}$. The distinction between the two types of superconductors may be drawn by means of the Ginzburg Landau parameter $\kappa = \frac{\lambda}{\xi}$, where ξ is the coherence length, representing the scale of spatial variation of the order parameter. If $\kappa < 1/\sqrt{2}$ the superconductor is said to be of type I, whereas for $\kappa > 1/\sqrt{2}$ it is of type II. For extreme type II superconductors, with $\kappa \gg 1$, the description is relatively simple when compared with the full Ginzburg-Landau picture. This condition is well satisfied in HTSC, and the cores of the flux lines (of radius ξ) can effectively be taken to be of zero extent. Therefore the field distribution of a single flux line can be described by an extended London equation:

$$\Delta\vec{B}(\vec{r}) - \frac{\vec{B}}{2\pi\lambda^2} = \frac{\Phi_0}{\lambda^2}\hat{z}\delta(\vec{r} - \vec{r}_0). \tag{4}$$

This equation has the well known solution

$$B_z(\vec{r}) = \frac{\Phi_0}{2\pi\lambda^2} K_0\left(\frac{\vec{r} - \vec{r}_0}{\lambda}\right), \tag{5}$$

where K_0 is the modified Hankel function of order zero [3]. From basic considerations, we can then get the energy density of the vortex line to be:

$$\epsilon_L \approx \frac{\Phi_0^2}{4\pi\mu_0\lambda^2} ln\left(\frac{\lambda}{\xi}\right). \tag{6}$$

The quadratic dependence of the energy on the flux quantum tells us that the flux line will contain only one quantum of flux. At intermediate fields $B_{c_1} \ll B_{ext} \ll B_{c_2}$ the field variation $B(\vec{r})$ of the flux line lattice will be periodic. It can therefore be expressed as a Fourier series:

$$B(\vec{r}) = \langle B \rangle \sum_{\vec{k}} b_{\vec{k}} \exp(i\vec{k}\vec{r}), \tag{7}$$

where $\langle B \rangle$ is the mean field within the superconductor. Introducing this as a solution into the modified London equation (Eq.(4)) one gets a solution for the Fourier components $b_{\vec{k}}$ as

$$b_{\vec{k}} = \frac{1}{1 + \lambda^2 |\vec{k}|^2}.$$

Thus the field distribution of a vortex lattice in the London limit is given by

$$B(\vec{r}) = \langle B \rangle \sum_{\vec{k}} \frac{\exp(i\vec{k}\vec{r})}{1 + \lambda^2 |\vec{k}|^2}, \tag{8}$$

where $\vec{k}$ are reciprocal vectors for a triangular lattice. As discussed above, however, the result of a μSR experiment is not the spatial field distribution B(r), but the field probability distribution p(B). For this reason we shall now consider the derivation of p(B) from B(r) for a vortex lattice. As already stated in Section 2,the field probability distribution is given by $p(B') := \langle \delta(B(\vec{r}) - B') \rangle$. For practical purposes however, it is more convenient to rewrite this as

$$p(B') = \frac{1}{L} \int \left(\left| \frac{\partial B(x,y)}{\partial y} \right| \right)^{-1} dx, \tag{9}$$

where the integration is carried out over lines of constant field $B(x, y) = B'$. This is the same procedure as a density of states calculation, but is carried out in two dimensions. At critical points (minima, maxima and saddle points) of the spatial field distributions, van Hove singularities thus occur. For a periodic field distribution, $p(B)$ vanishes outside the region $B_{min} < B < B_{max}$. At these minimum and maximum fields, the probability distribution exhibits jumps, while at saddle point fields B_{sad} a logarithmic divergence of $p(B)$ occurs. It can also be seen that due to the existence, close to the normal cores, of fields higher than the applied, the maximum field is much higher than the mean field. This leads to a highly asymmetric field probability distribution, which is shown schematically in fig 1.

Usually the second moment of the field distribution is extracted from μSR experiments by fitting a Gaussian relaxation function to the time signal. If it is assumed that the probability distribution is Gaussian, then the variance of the Gaussian σ is related to the second moment of the field distribution $\langle \Delta B^2 \rangle$ by $\sigma = \gamma_\mu \langle \Delta B^2 \rangle^{1/2}$. The latter is a direct measure of the penetration depth of the superconductor, which may be shown by deriving an expression for $\langle \Delta B^2 \rangle$ using the spatial distribution $B_z(r)$ derived earlier, yielding

$$\langle \Delta B^2 \rangle = \sum_{\vec{k}, |\vec{k}| \neq 0} \frac{B^2}{(1 + \lambda^2 |\vec{k}|^2)^2}. \tag{10}$$

In the limit $\lambda |\vec{k}| >> 1$, evaluation of the sum over all of the reciprocal lattice vectors for an hexagonal lattice gives $\langle \Delta B^2 \rangle = 0.00371 \Phi_0^2 / \lambda^4$ [5]. Refering to fig 1, however, it is clear that the field distribution is in general by no means Gaussian, raising doubts as to the validity of this approach. In polycrystalline samples of HTSC the lineshapes are often in fact roughly Gaussian, due to the effects of averaging over orientations of differing demagnetisation factors [6]. A study of powder samples in ref. [7] showed that experimentally σ and $\langle \Delta B^2 \rangle^{1/2}$ are proportional, so for studying systematic trends σ provides a good relative measure of the penetration depth [8] (this volume). For an absolute determination of λ, however, the actual second moment of the field distribution should be determined from the Fourier transform of the μSR time signal. For linewidths determined in this way there is a strong dependence on the statistics taken during the measurement. The very long tail in $p(B)$ at high fields becomes more significant relative to the noise with increasing statistics, hence the measured value of $\langle \Delta B^2 \rangle$ grows. As pointed out by Sidorenko *et al.* [9], in measurements on single crystals, the penetration depth can also be extracted from the value of

$$\langle B \rangle - B_{sad} = ln2 \frac{2}{3} \frac{\Phi_0}{4\pi\lambda_{ab}^2}, \tag{11}$$

where the mode of the distribution at B_{sad} is independent of statistics and $\langle B \rangle$ can be measured in magnetisation measurements. Even taking the value obtained for $\langle B \rangle$ from the μSR lineshape, the estimate of λ is less susceptible to the influence of statistics than if $\langle \Delta B^2 \rangle$ were used, since the distribution only enters linearly into the calculation. Comparing this with the above expression for $\langle \Delta B^2 \rangle^{1/2}$ for a perfect triangular lattice of extended vortex lines yields the parameter

$$\beta = (B_{sad} - \langle B \rangle) / \langle \Delta B^2 \rangle^{1/2} \simeq 0.6, \tag{12}$$

which can be used as a measure of the perfection of the flux lattice in the sample. Due to one or more of the above arguments the second moment is usually underestimated, so that the experimentally determined $\beta > 0.6$ for a perfect triangular lattice of rigid vortex lines.

In real vortex systems some degree of disorder will always exist. For instance non-periodic fluctuations of the internal field will arise from the spatial disorder induced in the lattice by random pinning sites. Distortions of a flux lattice composed of rigid vortex lines generally leads to a smearing of the field distribution, which convolutes the ideal-lattice field distribution with that due to the disorder [10]. These distortions are generally assumed to be of Gaussian form. Taking the most extreme case, for a random distribution of extended vortex lines, the second moment of the field distribution becomes [11]:

$$\langle \Delta B^2 \rangle = \frac{\Phi_0 B_{ext}}{4\pi\lambda^2}. \tag{13}$$

This linear dependence of $\langle \Delta B^2 \rangle$ on B is in strong contrast to case of an ideal lattice, where for intermediate fields $\langle \Delta B^2 \rangle$ is completely field *independent*. The flux lattice is, however, usually of sufficient order that these effects need not be taken into account. A case where this is not true will be discussed further in Section 4. Broadening of the field distributions due to nuclear moments may also occur. Usually this may also be neglected in superconductors, since the superconducting widths of the spectra (given by the value of the penetration depth) are approximately an order of magnitude broader than those arising from the nuclear moments. In superconductors with very long penetration depths, however, such as the organic charge transfer ET salts [12, 13, 14], the nuclear broadening is of the same order as the superconducting contribution to the linewidth. In that case the determination of the penetration depth from Eq.(11) is complicated, since the convolution shifts the peak field considerably. For this reason, in these compounds a reliable analysis requires that the contributions to the spectra from both the nuclear moments and the instrumental resolution must be deconvoluted from the measured lineshapes [13].

The above discussion is valid for isotropic superconductors. HTSC, in common with other systems such as organic superconductors or $NbSe_2$, show uniaxially anisotropic behaviour in their superconducting properties. This anisotropy arises from the highly layered structure of these compounds, yielding different values of the penetration depth for fields parallel and perpendicular to the superconducting planes. The anisotropy is parameterised by the ratio of the penetration depths due to currents flowing perpendicular and parallel to the planes $\gamma = \lambda_\perp/\lambda_\parallel$. In single crystals the second moment of the μSR field distribution is a measure of the average penetration depth perpendicular to the applied field. The second moment will therefore show an angular dependence, which takes the form

$$\langle \Delta B^2 \rangle(\vartheta) = \langle \Delta B^2 \rangle(0)(cos^2(\vartheta) + \gamma^{-2} sin^2(\vartheta)), \tag{14}$$

where γ is the anisotropy parameter and ϑ is the angle between the applied field and the axis perpendicular to the planes [15, 16, 17, 18]. In systems of moderate anisotropy, such as the HTSC $YBa_2Cu_3O_{7-\delta}$ (YBCO), it is possible to determine the anisotropy parameter. This was carried out by Forgan *et al.* [15] and is shown in fig. 2, yielding $\gamma \approx 5$. The extremely anisotropic HTSC $Bi_2Sr_2CaCu_2O_{8+\delta}$ (BSCCO), however, was not found to obey this relation at all applied fields [18]. It seems likely that these discrepancies arise due to the disorder of the vortices in this quasi-2D system, which is discussed further below. It is worth noting that for polycrystalline samples of anisotropic materials with $\gamma \gtrsim 5$, the value of the second moment of the field distribution is given by $\langle \Delta B^2 \rangle = 0.00371 F \Phi_0^2/\lambda_\perp^4$, where $F \approx 0.44$ [19]. That is, the polycrystalline average is *independent* of γ.

For extremely anisotropic superconductors such as the HTSC $Bi_2Sr_2CaCu_2O_{8+\delta}$ (BSCCO), the vortices are best described as a stack of quasi two-dimensional (2D) 'pancake' vortices, each confined to a superconducting plane. This opens another degree of freedom for disorder, since in such compounds vortex lines can be disordered along their length. In contrast to the case of disorder in a system of rigid vortex lines, the width of the μSR line is now *decreased*, since there is an effective smearing of the core fields due to the positional fluctuations [20]. This leads to a truncation of the long high field tail in the field distribution and hence to a narrower line. The nature of this disorder may be static (pinning-induced) or dynamic (thermally-induced). These fluctuations of the vortex positions can be taken into account in the determination of the width of the μSR line, by introducing a Debye-Waller type of factor into the expression given in Eq.(10), yielding [21, 22]

$$\langle \Delta B^2 \rangle = \sum_{\vec{k}} B^2 \frac{exp(-k^2\langle u^2 \rangle)}{(1+\lambda^2|\vec{k}|^2)^2}. \tag{15}$$

This is valid for both static and dynamic disorder, so long as the timescale for vortex motion is much greater than the timescale of the measurement. This is certainly realised in the HTSC, so that it is the time average of the

dynamic fluctuations which may be probed. For the highly anisotropic superconductor BSCCO the temperature dependence of the second moment has been studied in this respect by Lee *et al.* [23, 24]. Using theoretical calculations for the thermal fluctuations appropriate for highly anisotropic superconductors, as given by Blatter *et al.* [25], they were able to describe the field and temperature dependence of the second moment of the μSR lineshapes. In fig. 3 the form of the temperature dependence of the second moment is shown to be a strong function of applied field. The solid lines are calculations based on Eq.(15), only using parameters obtained independently, and are in excellent agreement with the data. The theory is even able to describe the anomalous migration from one curve to another at low fields [24]. It is thus clear that in highly anisotropic superconductors, the temperature dependence of the second moment of the field distribution does not necessarily reflect only the temperature dependence of the penetration depth. On the contrary, it may be strongly influenced by thermal fluctuations of pancake vortices, as in BSCCO.

The observations of the influence of thermal fluctuations discussed above where performed in a region of the magnetic phase diagram where the vortices essentially form strings of pancakes which resemble vortex lines. At these low fields the energetic cost of a shear deformation of the vortex lattice, due to the distortion introduced by the pinning site, is smaller than that of a local tilt of the line. The lattice can thus still be considered as consisting of extended lines. At higher fields the cost of shear deformations increases, and so local tilting of the vortex lines becomes more likely. The elastic moduli of the vortex lattice in HTSC are highly dispersive. At fields above that at which the dominant wavelength for tilt deformations becomes of the order of the inter-layer spacing of the superconducting planes s, the lattice may be regarded as crossing over to a more two-dimensional regime. For a strongly Josephson coupled layered superconductor this occurs at fields above $B_{2D} = \Phi_0/(\gamma s)^2$ [26, 27]. A similar crossover in behaviour is observed by μSR, where for field-cooled measurements at low temperature, the second moment is reduced drastically at a crossover field B_{cr} [28, 29]. Accompanying this reduction in width, a change in *lineshape* is also observed, producing a more symmetric field distribution. This is attributed to the static distortions induced on this softening lattice by random pins. These smear the fields associated with the vortex cores, leading to a strong reduction in the maximum field and hence a cut-off of the high field tail of the field distribution. Small angle neutron scattering (SANS) measurements by Cubitt *et al.* [30] concur with this interpretation, where the scattered neutron intensity dramatically drops above the same applied field.

This has been used by Bernhard *et al.* [31] to determine the anisotropy parameter for highly over- and underdoped BSCCO. It has however been shown recently [29], that this picture does not fully apply for superconductors as anisotropic as BSCCO, for which $\gamma s > \lambda_{\|}$. In that case at the field B_{2D} the inter-vortex separation, $a_0 = \sqrt{\Phi_0/B}$ is still bigger than the penetration depth, meaning that the vortices are only very weakly interacting. Therefore the crossover field is shifted to a value of

$$B_{cr} = \Phi_0/\lambda_{\|}^2, \tag{16}$$

above which the vortices begin to strongly overlap. This can be seen in fig. 4, where the crossover field as determined from μSR, or magnetisation measurements using the fishtail effect [29, 34], is shown as a function of the inverse square of the penetration depth. From that figure it can be clearly seen that the relation 16 is well observed in highly anisotropic superconductors. Similar results are also obtained in the organic superconductors [13], where the anisotropy is estimated to be of a similar order of magnitude as in BSCCO from magnetic torque measurements [35]. The determination of γ from measurements of the crossover field in extremely anisotropic superconductors does not, therefore, give the correct value, but rather a lower limit. The anisotropy of BSCCO can, however, be determined from μSR by another method, which we discuss below.

The high anisotropy of the samples results in highly flexible vortex lines. Combined with high transition temperatures, this results in the large thermal fluctuations discussed above. At sufficiently high temperatures the vortex lattice can acutally melt. Such a melting transition has been observed by many different techniques, such as resistivity [36, 37], magnetization [38, 39], specific heat [40], latent heat [41], SANS [30] and μSR [28, 24] in several HTSC compounds, such as YBCO and BSCCO. Recent latent heat measurements on detwinned single crystallite YBCO [41] give strong evidence for this to be a first order transition. In μSR the melting transition is observed by a sharp change in the shape of the field distribution, due to the truncation of the high field tail because of the smearing of the core fields [28, 24]. This change in shape can be seen in fig. 5, where two lineshapes, above and below the melting transition are shown. The line below the transition has a weighting to fields higher than the average, whereas above the transition the converse is true. This is shown by a change in sign of the lineshape asymmetry parameter

$$\alpha = \frac{\sqrt[3]{\langle \Delta B^3 \rangle}}{\sqrt{\langle \Delta B^2 \rangle}}. \tag{17}$$

The sharpness of the temperature dependence of α suggests the first order nature of the transition. This is shown in fig. 6, for an applied field of 30 mT. The melting temperature should be field dependent and can be estimated by a Lindemann criterion ($a_0^2 = c_L^2 \langle u^2 \rangle$). This gives a melting line in the magnetic phase diagram, which for instance could take the form

$$B_{3D}(T) \simeq \left[\frac{\Phi_0^5 c_L^4}{8\pi \mu_0^2 \gamma^2 k_B^2} \right] \left[\frac{1}{T^2 \lambda_\parallel^4(T)} \right], \tag{18}$$

which would allow a determination of the anisotropy parameter γ to be made. As in the calculation of B_{2D}, this does not take into account the extreme anisotropy of BSCCO. Blatter *et al.* [25] have recently reevaluated the determination of the melting line including electromagnetic interactions between pancake vortices in their calculations. According to this analysis, over large portions of the phase diagram the melting line is *independent* of the anisotropy if $\gamma s > \lambda_\parallel(T)$. This is satisfied up to a characteristic temperature T^{em} determined by

$$\lambda_\parallel(T^{em}) = \gamma s \tag{19}$$

where a crossover in the temperature dependence of the melting line occurs. The form of the melting line then changes from a $(T\lambda_\parallel^4(T))^{-1}$ to a $(T\lambda_\parallel^3(T))^{-1}$ behaviour. A similar crossover behaviour was observed in a μSR experiment [24], but with a change from a $(T\lambda_\parallel^4(T))^{-1}$ to a $(T\lambda_\parallel^2(T))^{-1}$ dependance. This is predicted for a simultaneous or closely separated melting and decoupling transition, which is also consistent with interpretations of data from other techniques such as SANS [30, 42]. The analysis leads to a value of $T^{em} = 70K$, and a corresponding $\gamma = 160$. In fig. 7 the melting line as determined from μSR is shown together with calculated curves based on ref. [25]. The Lindemann number c_L was determined from the low temperature part, whereas γ was determined from T^{em}. For this reason the high temperature part of the melting line has no adjustable parameters and is in excellent agreement with the experiment. As would be expected, the value of γ obtained in this way disagrees with that obtained by incorrectly identifying the crossover field with $B_{2D} = \Phi_0/(\gamma s)^2$.

Measurements of the temperature dependence of the penetration depth could reveal important information on the symmetry of the wavefunction of the Cooper pairs. For superconductors with strong coupling s-wave pairing a temperature dependence close to that of the phenomenological two-fluid model, given by

$$\lambda^2(T) = \frac{\lambda^2(0)}{1 - (T/T_c)^n}, \tag{20}$$

with $n = 4$, should be observed [7]. For d-wave coupling, however a linear temperature dependence at low temperature would be expected. The experimental μSR results are still somewhat inconclusive on this issue. For instance, a systematic study of powder samples of YBCO showed that as δ was varied the exponent in the phenomenological equation varied from $n \approx 2$ to $n \approx 4$ with increasing oxygen content [43]. Measurements on fully oxygenated single crystal YBCO, however, involving a full analysis of the μSR lineshape, gave evidence for a linear temperature dependence at low temperatures [44, 45]. It is not clear whether in this system the effects of thermal fluctuations should also be taken into account at high fields, in a manner similar to that discussed for BSCCO. If present these could certainly have an influence on the apparent temperature dependence of λ. In BSCCO the effects of thermal fluctuations are so influential, that the authors doubt whether the dependence of $\lambda(T)$ may be sufficiently well determined by μSR to distinguish s-wave from d-wave coupling.

4 Pinning of flux lines

The pinning of flux vortices can arise most commonly from metallurgical defects in the sample at which the superconductivity is partially or wholly supressed. To be effective, such a pinning site has to extend at least over a volume of ξ^3, where ξ is the coherence length, since changes in the order parameter can only take place over ξ. The gain in energy by the pinning of a flux line can be estimated as

$$E_{pin} = \frac{B_c^2 \xi^3}{2\mu_0} = \frac{\Phi_0^2 \xi}{16\pi^2 \mu_0 \lambda^2}, \tag{21}$$

where $B_c = \Phi_0/(2\sqrt{2}\pi\xi\lambda)$ is the thermodynamical critical field. In the case of an applied current, for perfect conductivity to break down, the force exerted on the vortices from these pinning sites has to be matched by the Lorentz force due to the current. Depinning can also arise, however, due to thermal motion. In that case the pinning energy has to be matched by the thermal energy $k_B T_{dp}$, such that pinning becomes ineffective.

The above estimate yields a value of $T_{dp} \simeq 30K$ in the HTSC BSCCO. It has been suggested, from SANS [42] and magnetisation measurements [46, 47] , that this is indeed a reasonable estimate. In magnetisation measurements one observes a sharp increase in zero field cooled magnetization, indicating a sudden penetration of magnetic flux into the sample [46, 47]. This is possible at the depinning transition, since the mobility of the flux lines increases and therefore they are more easily redistributed within the sample. More convincingly in SANS a reemergence of a scattering signal from a flux line lattice has been observed for temperatures above 25 K and applied fields higher than the crossover field B_{cr} [42]. As discussed in the previous section, the crossover field is thought to be manifest due to the accomdodation of the flux lines to the pinning sites, arising from the increasing flexibilty of the vortices. It appears that with increasing temperature the vortices depin and briefly become *more ordered* along their length. As temperature increases further thermally-induced disorder eventually increases to the point that the lattice melts or decouples [24, 42]. We have recently observed a depinning transition in single crystal BSCCO samples using μSR. By cooling the sample in an applied field greater than the crossover field, we effectively produced a vortex glass of mean spacing $a_0^{freeze} = \sqrt{\Phi_0/B_{ext}^{(a)}}$. The strongly pinned nature of the vortex distribution is verified by the fact that the field distribution within the sample is not changed by application, at low temperatures, of another field. This can be seen in fig. 8, where the μSR line is shown for a sample cooled to 5 K in a field of 90 mT and changed to 75 mT at 5 K. On raising the temperature, the thermal energy starts to become comparable to the pinning energy and flux lines begin to become more mobile. This leads to a redistribution of the vortex lattice around the newly applied field $B_{ext}^{(b)}$. This is apparent in the μSR signal as two peaks, one at the first field $B_{ext}^{(a)}$ the other at the present field $B_{ext}^{(b)}$. A series of μSR lines for such an experiment is shown in fig. 8, for a frozen field of 90 mT. The depinning temperature is $T_{dp} \simeq 28K$ in accordance with SANS and magnetisation measurements. In fig. 8 the μSR lines are normalised to their peak value for clarity. In the experiment a distinct drop in muon asymmetry is observed, due to a very broad distribution of fields leading to fast depolarisation effects which occur at short times outside of the time window of the experiment [48].

To raise critical currents in HTSC, the anisotropic strong pinning sites may be introduced, which are produced by the irradiation of the samples with fast heavy ions. The changes introduced to the magnetic phase diagram by these columnar defects have been studied intensely over the past years [49, 50, 51, 52, 53, 54]. Since the irradiation of the samples is completely random, the flux distribution expected for such a sample is close to a random arrangement discussed earlier, except for some correlations due to interactions between the vortices [55, 56]. Furthermore, since the defects extend over the whole sample, the columnar defects also increase the dimensionality of the vortex system, in that they effectively confine the fluctuations of pancake vortices to within the extent of the defect [57]. As in unirradiated samples, we have also probed the depinning temperature of samples containing columnar defects by μSR. Magnetisation measurements suggest a significantly higher depinning temperature from the columnar defects [47]. A series of experiments as described above is shown for an irradiated sample in fig. 9. The signatures of depinning are the same as for unirradiated samples, but the depinning temperature is significantly higher, $T_{dp} \simeq 55K$. This is in good agreement with the results from magnetisation measurements on the same sample [47]. The value of the μSR data is that it provides additional information on the microscopic arrangement, such as the growth of domains around different average internal field values. These results will be discussed in more detail elsewhere [47, 48].

5 Conclusions

We have shown that transverse field μSR presents an excellent tool for the investigation of the phenomenology of the vortex lattice in type II superconductors. Thermal and static fluctuations in the vortex positions are readily observed, leading to the observation of flux-line lattice melting. There is a clear distinction possible between 3D (line-like) and 2D disorder, making it possible to observe the dimensionality of the vortex system. In highly anisotropic superconductors this has led to the observation of a dimensional crossover field. We have also shown, how μSR can be used to investigate microscopically the important phenomenon of pinning in type II superconductors.

With knowledge of the phenomenology of the vortex lattice it is also possible to use μSR for investigations of fundamental superconducting properties, such as the pairing symmetry or the value of the magnetic penetration depth. From systematic studies of several classes of superconductors, new insights are gained on their microscopic nature (see also ref. [8]).

6 Acknowledgements

We would like to acknowledge the collaboration with E. M. Forgan, R. Cubitt, H. Keller, R. Cywinski, B. Stäuble-Pümpin, A. D. Hillier, S. H. Lloyd, P. Zimmermann, M. Warden, M. B. Hunt, C. Ager, F. L. Pratt, S. J. Blundell, I. M. Savić. This work was supported by the Swiss National Science Foundation and the EPSRC of the United Kingdom.

References

[1] E. Roduner, this volume.

[2] B. D. Rainford, G. J. Daniell, Hyperfine Interactions **87**, 1129 (1994).

[3] M. Tinkham, Introduction to Superconductivity (McGraw-Hill, 1975).

[4] E. H. Brandt, A. Seeger, Adv. in Physics **35**, 189 (1986).

[5] see e.g. E. H. Brandt, Phys. Rev. B **37**, 2349 (1988).

[6] M. Weber *et al.*, Phys. Rev. B **48**, 13022 (1993).

[7] B. Pümpin *et al.*, Phys. Rev. B **42**, 8019 (1990).

[8] R. Cywinski and A. Hillier, this volume.

[9] A. D. Sidorenko, V. P. Smilga, V. I. Fesenko, Hyperfine Interactions **63**, 49 (1990); A. D. Sidorenko, V. P. Smilga, V. I. Fesenko, Physica C **166**, 167 (1990).

[10] E. H. Brandt, J. of Low Temp. Physics **73**, 355 (1988).

[11] V. N. Belusov *et al.*, Usp. Fiz. Nauk **160**, 55 (1990).

[12] S. L. Lee *et al.*, *Proc. Int. Conf. on Science and Technology of Synthetic Metals (Snowbird,1996);* Synth. Met. **85/1-3** (1996).

[13] S. L. Lee *et al.*, submitted to Phys. Rev. Lett. (1996).

[14] S. J. Blundell *et al.*, this volume.

[15] E.M. Forgan *et al.*, Hyperfine Interactions **63**, 71 (1990).

[16] V. I. Fesenko *et al.*, Physica C **176**, 551 (1991).

[17] S.L. Thiemann *et al.*, Phys. Rev. B **39**, 11406 (1989).

[18] R. Cubitt *et al.*, Physica C **213**, 126 (1993).

[19] W. Barford and J.M.F. Gunn, Physica C **156**, 515 (1988).

[20] E. H. Brandt, Phys. Rev. Lett. **66**, 3213 (1991).

[21] Y.-Q. Song *et al.*, Phys. Rev. Lett. **70** 3127 (1993); Y.-Q. Song *et al.*, Physica **C 241**, 187 (1995).

[22] D.R. Harshmann *et al.* Phys. Rev. Lett. **61**,3152 (1995).

[23] S. L. Lee *et al.* Phys. Rev. Lett. **75**,922 (1995).

[24] S. L. Lee *et al.* Phys. Rev. B **55**(6) (1997).

[25] G. Blatter *et al.*, Phys. Rev. B **54**, 72 (1996).

[26] L. I. Glazman, A. E. Koshelev, Phys. Rev. B **43**, 2835 (1991).

[27] G. Blatter *et al.* Rev. Mod. Phys. **66**, 1125 (1995).

[28] S. L. Lee *et al.*, Phys. Rev. Lett. **71**, 3862 (1993).

[29] C. M. Aegerter *et al.* Phys. Rev. B **54**, R15661 (1996).

[30] R. Cubitt *et al.*, Nature **365**, 407 (1993).

[31] C. Bernhard *et al.*, Phys. Rev. B **52**, R7050 (1995).

[32] B. Khaykovich *et al.* Phys. Rev. Lett. **76**, 2555 (1996).

[33] V. N. Kopylov *et al.*, Physica C **170**, 291 (1990).

[34] G. Yang *et al.* Proceedings of the 7th International Workshop on Critical Currents in Superconductors, Alpbach, Austria; edited by H. W. Weber (1994).

[35] P. A. Mansky *et al.* Phys. Rev. B **50**, 15929 (1994).

[36] W. K. Kwok *et al.*, Phys. Rev. Lett. **72**, 1092 (1994).

[37] D. T. Fuchs *et al.* Phys. Rev. B **54**, R796 (1996).

[38] H. Pastoriza *et al.* Phys. Rev. Lett. **72**, 2951 (1994).

[39] E. Zeldov *et al.* Nature **375**, 373 (1995).

[40] M. Roulin *et al.* Science **273**, 1210 (1996).

[41] A. Schilling *et al.* Nature **382**, 791 (1996).

[42] S. H. Lloyd, C. M. Aegerter, in preparation (1997).

[43] P. Zimmermann *et al.*, Phys. Rev. **B 52**, 541 (1995).

[44] J. E. Sonier *et al.*, Phys. Rev. Lett. **72**, 744 (1994).

[45] T. M. Riseman *et al.*Phys. Rev. **B 52**, 10569 (1995).

[46] H. Pastoriza *et al.*, Phys. Rev. B **46**, 9278 (1992).

[47] C. M. Aegerter *et al.*, submitted to Physica C (1997).

[48] C. M. Aegerter *et al.*, in preparation.

[49] V. M. Vinokur, D. R. Nelson Phys. Rev. Lett. **68**, 12398 (1992); Phys. Rev. B **48**, 13060 (1993).

[50] L. Civale *et al.* Phys. Rev. Lett.**67**, 648 (1991); L. Krusin-Elbaum *et al.* Phys. Rev. Lett. **72**, 1914 (1994).

[51] V. Hardy *et al.* Physica C **191**, 85 (1992).

[52] D. Zech *et al.* Phys. Rev. B **52**, 6913 (1995).

[53] D. Zech *et al.* Phys. Rev. B **54**, (1996).

[54] V. V. Moshalkov *et al.* Phys. Rev. B **50**, 639 (1994).

[55] U. C. Täuber and D. R. Nelson, Phys. Rev. B (1996).

[56] S. H. Lloyd *et al.* to be published.

[57] C. M. Aegerter *et al.*, to be published.

Figure 1: Field probability density $p(B)$ at four different temperatures. At T=0 the van Hove jumps at B_{min} and B_{max} disappear due to the appearance of cusps in $B(x, y)$. Figure according to ref [4].

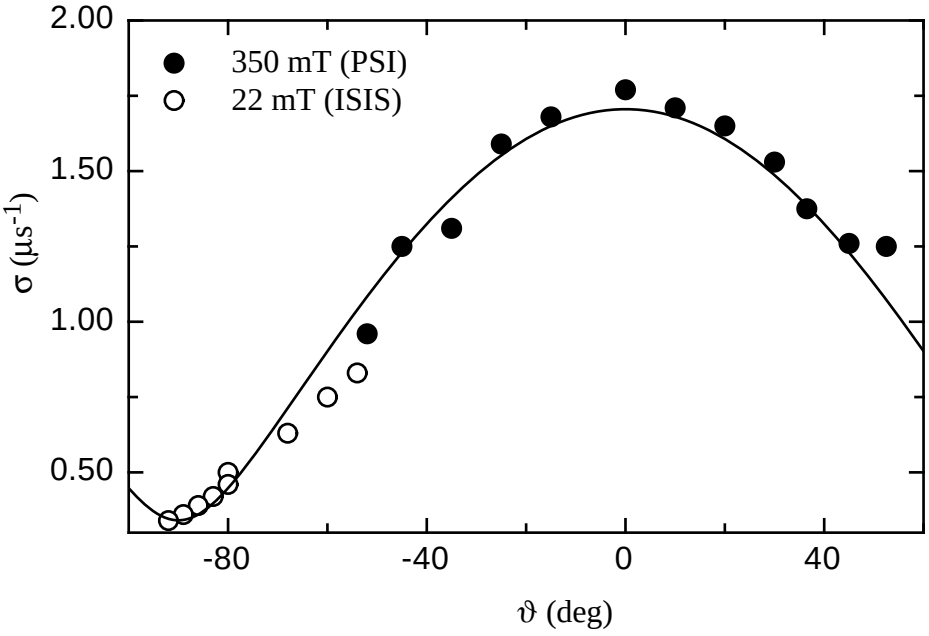

Figure 2: The angular dependence of the μSR relaxation rate for a single-crystal sample of YBCO. As discussed in the text, the relaxation rate is assumed to be Gaussian, and is proportional to the second moment of the local field distribution. This quantity is a measure of the inverse square of the penetration depth and follows an angular dependence as given in Eq. (14). The dashed line is a fit to this function resulting in a value of $\gamma = 5$.

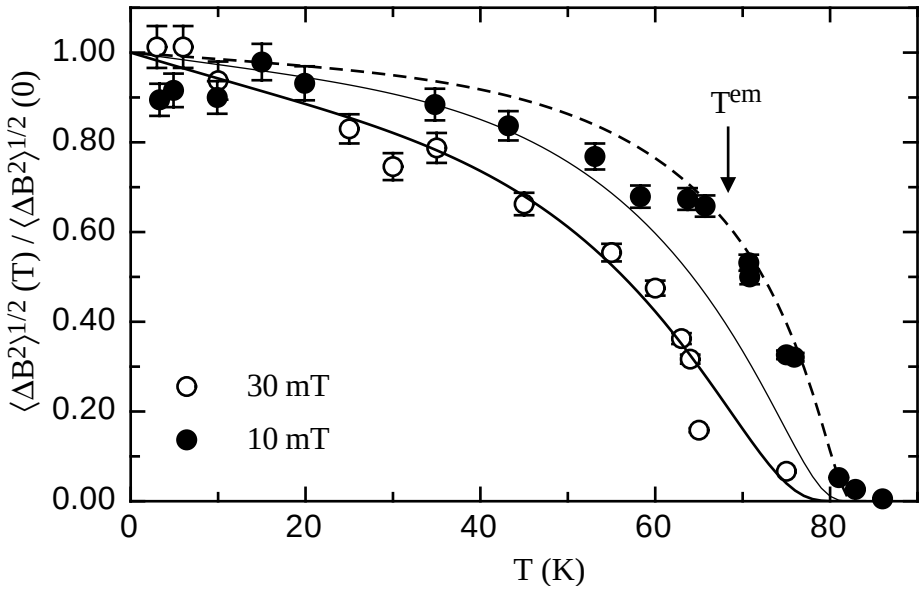

Figure 3: Measurements taken from Ref. [23] of the μSR-linewidths $\langle(\Delta B)^2\rangle(B,T)$ in BSCCO at fields of 10mT (filled circles) and 30mT (empty circles). For $T < T^{em}, T_m$ the data are described without *any adjustable parameters* by Eq. (15), using the appropriate expression for vortex fluctuations in this region, $\langle u^2_{em}\rangle^{1/2}(B,T)$ [25] (solid curves). The dashed line is the expected curve for $T^{em} < T < T_m$ at 10mT, using $\langle u^2_{em,J}\rangle(B,T)$ [25]. The 10mT data migrates towards this curve for temperatures above T^{em}, reflecting the crossover illustrated in Fig. 7.

Figure 4: The crossover field B_{cr} as a function of $\lambda_{ab}^{-2}(0)$ for different samples of BSCCO. Open symbols correspond to μSR measurements on samples studied in ref. [29]: circle is sample S_1; square S_2; diamond S_3. Filled diamonds are taken from ref. [32] and are obtained from magnetisation measurements using Hall bar arrays. The filled circle is from a Tl-2212 sample taken from ref. [33], where the crossover field is determined by magnetisation measurements. The solid line corresponds to the relation $B_{cr} = \Phi_\circ/\lambda_{ab}^2$, which describes the data without any adjustable parameter.

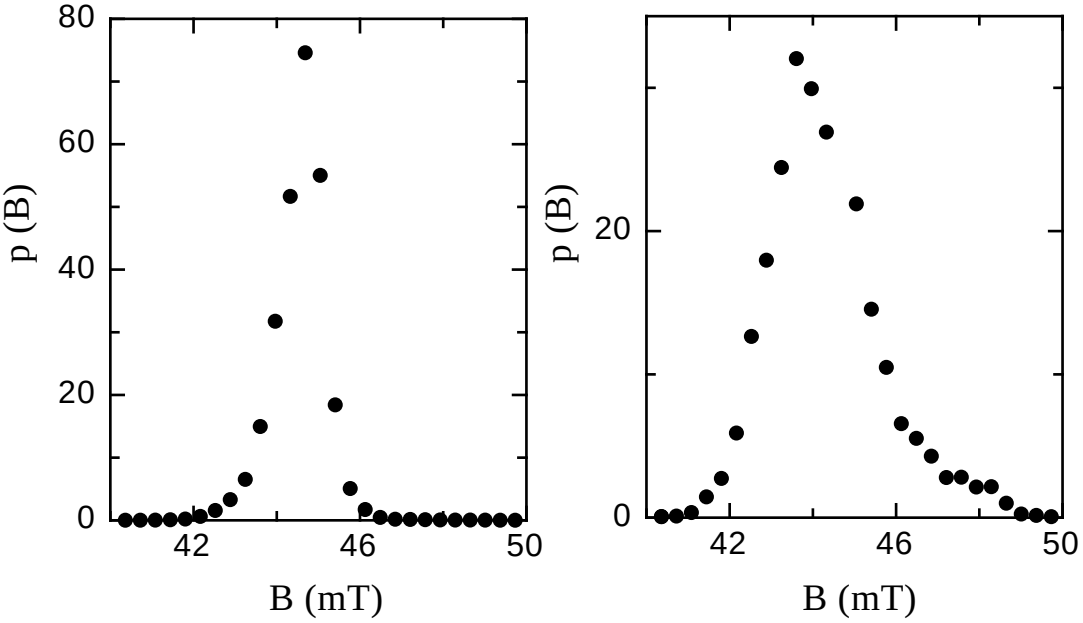

Figure 5: μSR lineshapes for BSCCO in an applied field of 45 mT. On the right the line shape is shown at 46 K, below the melting transition T_m, on the left it is shown at 68 K, above the transition.

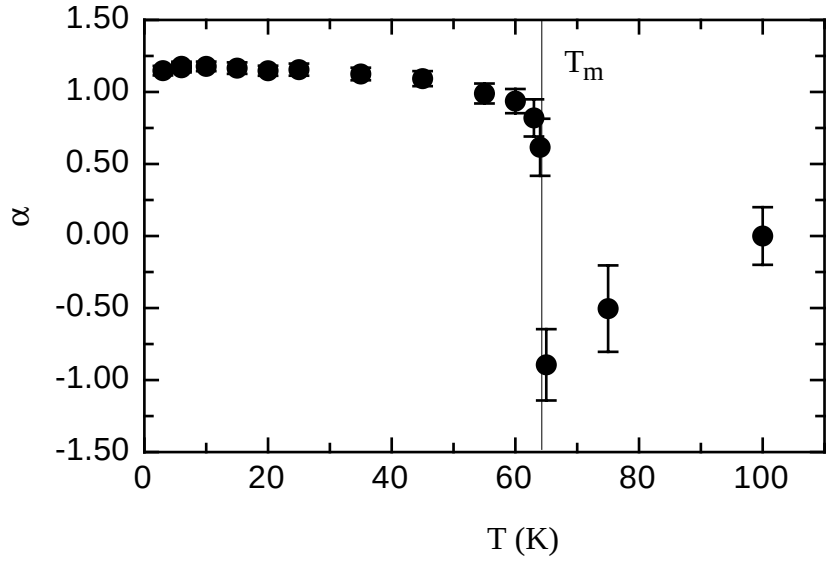

Figure 6: The skewness of the μSR-lineshape may be represented by a quantity α derived from the third and second moments of the probability distribution $p(B)$ (see text). The lineshape and corresponding α observed below the transition temperature T_m are characteristic of a vortex-line lattice, the disappearance of which is indicated by the sharp change of α at T_m [28, 24]. These data are field cooled measurements for an applied field of 30mT.

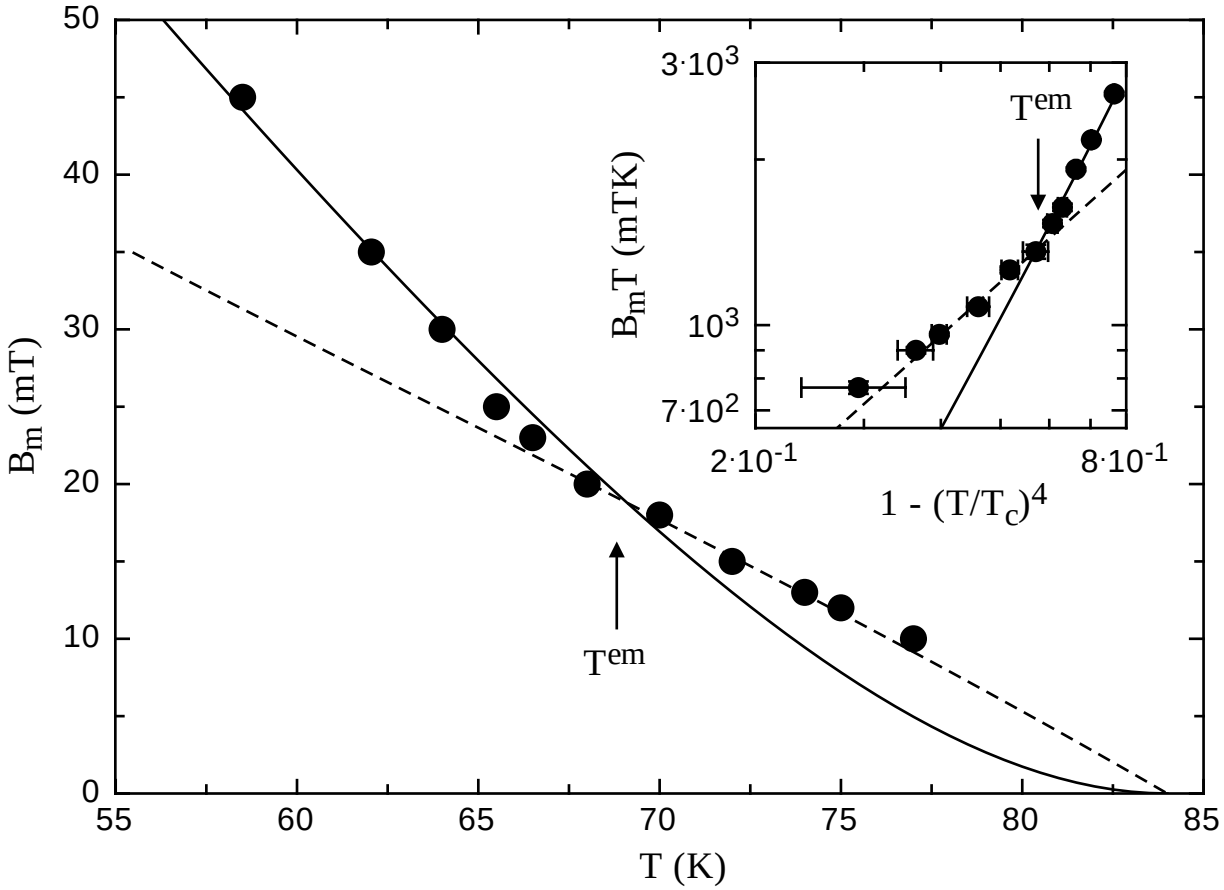

Figure 7: Measurements taken from Ref. [24] of the phase line $B_m(T)$. This represents the transition of the vortex lattice in BSCCO as determined by changes in the μSR-lineshape, such as those represented in Figure 6. Note the change in the curve at temperature T^{em} . The solid curve is a fit of the data, for $T < T^{em}$, to the melting curve Eq.(1) of ref. [24] with $c_L = 0.18$, or alternatively a fit to the decoupling curve Eq.(4) of ref. [24] with $c_D = 0.076$. In this region, electromagnetic coupling between pancake vortices in adjacent superconducting layers is the dominant interaction. The dashed line is the decoupling function Eq.(3) of ref. [24], with c_D taken from above, and a value of $\gamma = 160$ taken from the position of T^{em} (see text). The inset is a logarithmic plot of the data and fitted curves.

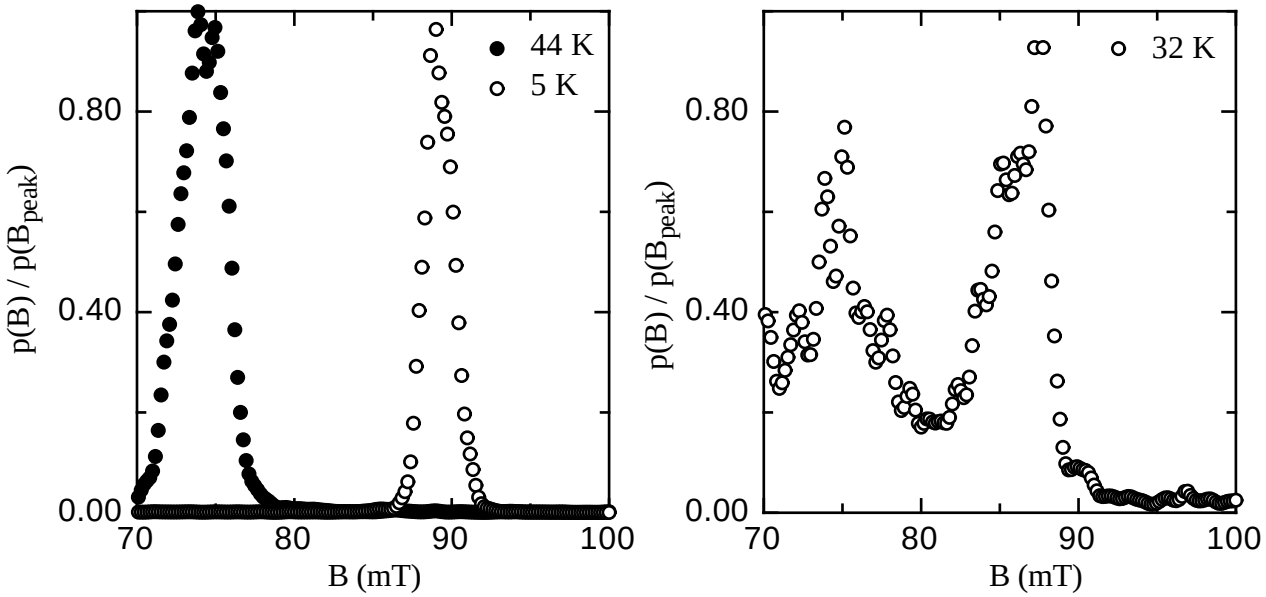

Figure 8: Field distributions in BSCCO for different temperatures. The spectra were taken after cooling the samples to 5 K in an applied field of 90 mT. A field of 75 mT was subsequently applied. That the field distribution is not changed indicates strong pinning in this field and temperature range. As the temperature is raised, the mean internal field changes from 90 mT to 75 mT in the range 25-40K. This reflects a thermal depinning of vortices and is in accord with the recent observation of a reemergance of Bragg peaks in SANS for the same temperature and field [42].

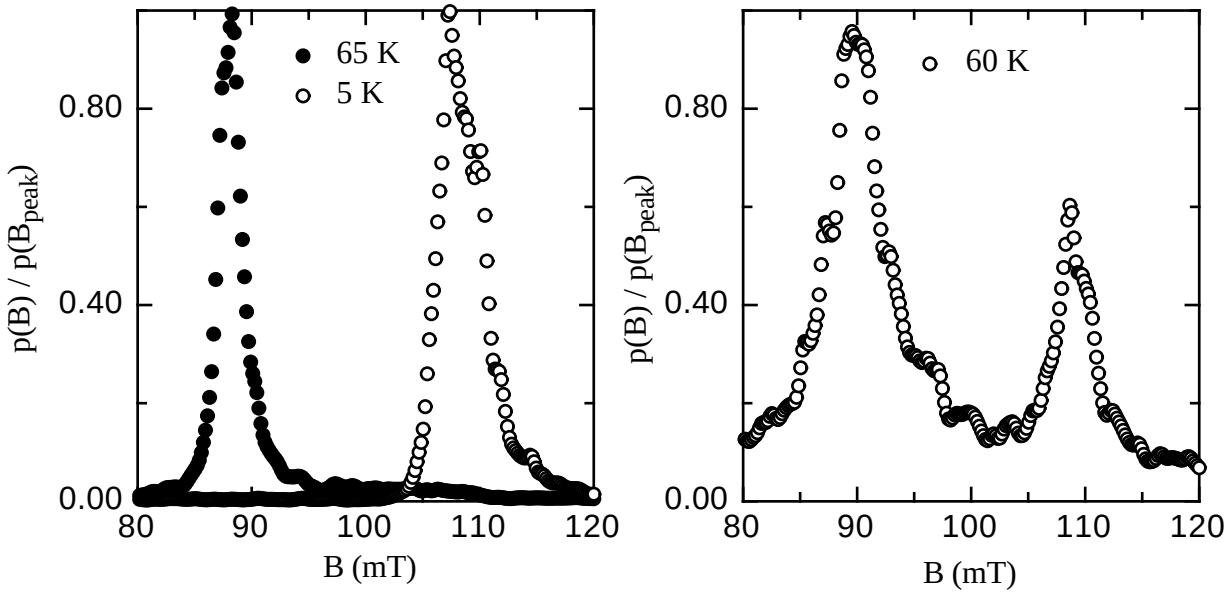

Figure 9: The field distribution for a sample containing columnar defects at different temperatures. The spectra were taken after cooling the samples to 5 K in an applied field of 110 mT. The field was subsequently decreased to 90 mT and the sample temperature raised. For temperatures in the range of 55 - 60 K, the mean internal field changes from the value of the frozen field (110 mT) to the applied (90 mT). The value of the depinning temperature thus obtained is in good agreement with that obtained from magnetisation measurements [47].